Ukrainian Journal of Physical Optics
ISSUE 2
2026

ELECTRONIC, OPTICAL, AND VIBRATIONAL PROPERTIES OF LAYERED $In_{0.3}Ga_{0.7}Se$: A DFT AND RAMAN STUDY

K.K. AZIZOVA [1,2], Z.A. JAHANGIRLI [1,3], T.K. NURUBEYLI *[1,4,5], L.CH. SULEYMANOVA [6], A.H. SULTANOVA [7], N.V. KERIMLI [8], S.O. GULIEVA [9], S.S. OSMANOVA [10], L.V. MAMMADOV [11], N.V. KAZIMOVA [12]

[1] Institute of Physics of the Ministry of Science and Education of the Republic of Azerbaijan, H. Javid Ave., 131, Baku, AZ-1073, Azerbaijan
[2] Western Caspian University, 21 Ahmad Rajabli, Baku, AZ-1072, Azerbaijan
[3] Baku State University, Zahid Khalilov Str., 23, Baku, AZ-1148, Azerbaijan
[4] Azerbaijan State Oil and Industry University, Azadliq Avenue, 20, Baku, AZ-1010, Azerbaijan
[5] Khazar University, Mahsati Str. 41, Baku, AZ 1096, Azerbaijan
[6] Mingachevir State University, 21 D. Aliyeva Str., Mingachevir, AZ-4500, Azerbaijan
[7] Nakhchivan State University, A. Aliyev 11, AZ-7000, Nakhchivan city, Azerbaijan
[8] Azerbaijan Medical University, Samad Vurgun Str.167, Baku AZ-1022, Azerbaijan
[9] The Academy of Public Administration under the President of the Republic of Azerbaijan, 74 Lermontov Str., Baku, AZ-1001, Azerbaijan
[10] Azerbaijan Technical University, H.Javid Ave. 25, Baku, AZ-1073, Azerbaijan
[11] Baku Engineering University, Hasan Aliyev Str. 120, Khirdalan city, AZ-0101, Absheron, Baku, Azerbaijan
[12] Azerbaijan Technological University, 103 Shah Ismayil Khatai Ave., AZ-2011 Ganja, Azerbaijan
*Corresponding author: omartarana@gmail.com

Received: 06.01.2026

Abstract. The electronic structure, optical response, and vibrational properties of the $In_{0.3}Ga_{0.7}Se$ crystal were investigated using first-principles density functional theory. The dielectric tensor components were calculated, enabling a detailed analysis of the refractive index, extinction coefficient, absorption coefficient, optical conductivity, and reflectivity for light polarized parallel and perpendicular to the optical axis. The results identify $In_{0.3}Ga_{0.7}Se$ as a direct-gap semiconductor with a fundamental band gap of 1.91 eV, highlighting its potential for optoelectronic applications in the visible spectral range. To elucidate the electronic structure, atom-projected partial densities of states were analyzed, revealing the contributions of In, Ga, and Se orbitals to the valence and conduction bands. The vibrational properties were examined through a combined theoretical and experimental approach using density-functional perturbation theory and Raman spectroscopy. A direct comparison between the calculated phonon modes and the experimental Raman spectrum allowed the assignment of five Raman-active modes at 40, 111, 180, 225, and 256 cm^{-1}, corresponding to A_1, B_1, E_2, and E_1 symmetry representations. The associated atomic displacement patterns were analyzed to clarify the nature of lattice vibrations in the mixed-cation system. In addition, the temperature dependence of the heat capacity was calculated over the range of 0–400 K, providing insight into the thermodynamic behavior of $In_{0.3}Ga_{0.7}Se$. The overall agreement between the calculated phonon frequencies and experimental Raman data confirms the reliability of the first-principles approach and establishes a consistent description of the electronic, optical, vibrational, and thermodynamic properties of this non-equiatomic In–Ga–Se solid solution.

Keywords: $In_{0.3}Ga_{0.7}Se$ crystals, density functional theory, electronic structure, optical anisotropy, Raman spectroscopy, phonon properties
UDC: 538.958
DOI: 10.3116/16091833/Ukr.J.Phys.Opt.2026.02043

1. Introduction

Layered III–VI chalcogenide semiconductors have recently regained interest due to their notable structural anisotropy, adjustable electronic band structure, and strong light–matter interactions. These qualities make them promising for next-generation optoelectronic and photonic devices

[1–3]. Specifically, materials like indium selenide (InSe) and gallium selenide (GaSe) feature direct band gaps within the visible spectrum, high absorption coefficients, and significant optical anisotropy, supporting applications in photodetectors, nonlinear optics, and energy-conversion systems [4–6].

Beyond binary compounds, solid solutions based on the In–Ga–Se system offer an effective way for band-gap engineering and tailoring optical and vibrational properties through controlled cation substitution. Recent experimental and theoretical studies have shown that adjusting composition in layered chalcogenides can greatly alter dielectric response, carrier transport, and lattice dynamics, thus broadening their functional versatility [7–9]. However, compared to the extensive research on binary InSe and GaSe, In–Ga–Se solid solutions are still much less studied, especially for non-equiatomic compositions [10].

From a theoretical standpoint, first-principles density functional theory (DFT) has been extensively used to study the electronic and optical properties of layered chalcogenides, offering valuable insights into band dispersion, optical anisotropy, and bonding characteristics [11–13]. Recent DFT-based research has also emphasized the significance of vibrational properties and phonon-related thermodynamic quantities in evaluating lattice stability and thermal behavior, which are essential for practical device operation [14,15]. However, comprehensive studies that combine electronic structure, optical response, lattice dynamics, and thermodynamic properties within a single framework are still limited for In–Ga–Se solid solutions.

In particular, the non-equiatomic composition $In_{0.3}Ga_{0.7}Se$ represents an intermediate substitution regime where the relative contributions of In and Ga cations are expected to strongly influence both the electronic band structure and phonon spectra. Understanding how this specific composition affects band-gap properties, optical anisotropy, Raman-active phonon modes, and heat capacity is crucial for assessing its potential in optoelectronic applications within the visible spectrum. Additionally, experimental validation of vibrational properties through Raman spectroscopy offers an important benchmark for theoretical predictions and improves the reliability of first-principles modeling.

In this work, we provide a thorough investigation of the electronic, optical, vibrational, and thermodynamic properties of the $In_{0.3}Ga_{0.7}Se$ crystal using first-principles calculations complemented by Raman spectroscopy. The electronic structure and optical response are examined with the full-potential linearized augmented plane-wave method, with particular focus on optical anisotropy. Lattice dynamics are analyzed within density-functional perturbation theory, allowing for direct comparison between calculated phonon modes and experimental Raman spectra. Additionally, the temperature dependence of the heat capacity is assessed to understand the thermodynamic behavior of this material. This study addresses a key gap in the understanding of non-equiatomic In–Ga–Se solid solutions and offers a reliable reference for future experimental and theoretical research.

Despite increasing interest in In–Ga–Se solid solutions, their polarization-dependent optical response and dielectric anisotropy remain underexplored, especially for non-equiatomic compositions. This motivates the current optical-focused first-principles and Raman study.

2. Computational details and experimental methods

First-principles calculations of the electronic structure and optical properties of $In_{0.3}Ga_{0.7}Se$ were performed using the full-potential linearized augmented plane-wave (FP-LAPW) method as implemented in the WIEN2k software package [16,17]. A plane-wave cutoff

parameter of $R_{mt}K_{max}$ = 7.0 was employed, and the potential and charge density inside the muffin-tin spheres were expanded in spherical harmonics up to a maximum angular momentum of l_{max} = 10. The muffin-tin radii for In, Ga, and Se atoms were all set to 2.0 Bohr. Core and valence states were separated using an energy threshold of −6.0 Ry.

Brillouin-zone integrations were carried out using a dense k-point mesh corresponding to approximately 2000 *k*-points in the full Brillouin zone, employing the tetrahedron method to ensure accurate convergence of the charge density and total energy [18,19]. Exchange–correlation effects were initially treated within the generalized gradient approximation (GGA) using the Perdew–Burke–Ernzerhof functional [20]. To obtain a more reliable description of the electronic band gap, subsequent calculations were performed using the modified Becke–Johnson (mBJ) exchange potential [21], which has been shown to provide improved band-gap predictions for semiconductors and layered materials.

Lattice dynamical properties were investigated within the framework of density-functional perturbation theory (DFPT) [22–24], as implemented in the ABINIT code [25]. Norm-conserving Hartwigsen–Goedecker–Hutter pseudopotentials were employed in combination with the GGA exchange–correlation functional [26-28]. A plane-wave kinetic-energy cutoff of 80 Ry was used to expand the electronic wavefunctions. Brillouin-zone sampling was performed using a 4×4×4 Monkhorst–Pack *k*-point mesh [29,30].

The experimentally reported layered crystal structure of $In_{0.3}Ga_{0.7}Se$ was used as the starting point for all calculations. The non-equiatomic composition was modeled using a supercell constructed to preserve layered symmetry while reflecting the target In/Ga ratio. Structural relaxation was carried out using the Broyden–Fletcher–Goldfarb–Shanno algorithm until the Hellmann–Feynman forces acting on each atom were less than 10^{-4} eV Å^{-1}. Prior to the final calculations, systematic convergence tests with respect to k-point density and plane-wave cutoff were performed to ensure the reliability and numerical accuracy of the results.

The $In_{0.3}Ga_{0.7}Se$ crystal belongs to the family of layered III–VI chalcogenides and crystallizes in a hexagonal structure with pronounced anisotropy between the in-plane and out-of-plane directions. In this crystallographic setting, the *a* and *b* axes lie within the basal plane of the layers, while the *c*-axis is oriented perpendicular to the layers and corresponds to the optical axis of the crystal.

Owing to the weak van der Waals bonding between adjacent layers, the natural cleavage plane is the (001) plane, which is parallel to the *ab* plane. Accordingly, optical properties were calculated by explicitly distinguishing the in-plane polarization ($E \perp c$, along the *a* and *b* directions) and the out-of-plane polarization ($E \parallel c$), allowing a direct assessment of optical anisotropy associated with the layered crystal structure.

Bulk $In_{0.3}Ga_{0.7}Se$ layered crystals were synthesized using a melt-based ampoule growth technique, following a procedure similar to that previously reported for In–Ga–Se solid solutions. High-purity elemental gallium (99.999 wt.%), indium (99.99 wt.%), and selenium (99.999 wt.%) were used as starting materials.

Stoichiometric amounts corresponding to the nominal composition $In_{0.3}Ga_{0.7}Se$ were weighed and sealed in evacuated graphite-coated silica ampoules under a residual pressure of approximately 10^{-3} Pa. Graphitization of the inner ampoule walls was achieved by thermal decomposition of acetone in order to prevent parasitic reactions with the silica.

Due to selenium's high vapor pressure, the ampoules were initially heated to

approximately 350°C and held at this temperature for 2 h to ensure a controlled reaction between selenium and the metallic components. Subsequently, the temperature was increased to 1000°C, and the melt was homogenized by periodic rocking of the furnace. After homogenization, the samples were slowly cooled down to 400°C and annealed at this temperature for two weeks to promote compositional uniformity and structural ordering. Finally, the ampoules were cooled to room temperature at a controlled rate [31]. The obtained ingots exhibited a layered morphology with well-defined cleavage planes parallel to the (0001) plane, typical of hexagonal III–VI chalcogenides.

Raman scattering measurements were performed at room temperature using a 3D confocal micro-Raman spectrometer (Nanofinder 30, Tokyo Instruments, Japan). A frequency-doubled Nd: YAG laser with an excitation wavelength of 532 nm was employed as the light source. The laser power at the sample surface was limited to 10 mW to avoid local heating. The diameter of the laser spot was approximately 4 μm [31]. The Raman spectra were recorded in a backscattering geometry from the freshly cleaved surface parallel to the (0001) plane. The scattered light was detected using a thermoelectrically cooled CCD detector operated at −70°C. All spectra were corrected for background contributions prior to analysis.

The phase composition and crystal structure of the grown $In_{0.3}Ga_{0.7}Se$ crystals were examined by powder X-ray diffraction (PXRD) at room temperature using CuKα radiation. The diffraction patterns were analyzed by the Rietveld refinement method. The obtained results confirmed that the samples crystallize in a hexagonal structure belonging to the $P6_3mc$ space group, with no detectable secondary phases within the experimental resolution.

3. Electronic structure and optical properties

It is well established that standard local and semi-local exchange–correlation functionals within the local density approximation tend to systematically underestimate the fundamental band gaps of semiconducting materials. This limitation arises from the incomplete cancellation of self-interaction errors and the absence of a proper derivative discontinuity in the exchange–correlation potential. In order to obtain a more reliable description of the electronic structure and optical response of the $In_{0.3}Ga_{0.7}Se$ crystal, the present study employs the modified Becke–Johnson (mBJ) meta-GGA exchange potential, which has been shown to significantly improve band-gap predictions for a wide range of semiconductors and layered materials.

It should be noted that the indium content of 30 at.% investigated in the present work significantly exceeds the maximum indium concentration reported for flux-grown crystals in Ref. Sato et al. [7]. This difference originates from the fundamentally different growth approach employed in this study. While flux-based traveling heater methods impose solubility limits on indium incorporation, the melt-based ampoule synthesis used here enables stabilization of higher indium concentrations in layered In–Ga–Se solid solutions, as previously demonstrated for $In_{1-x}Ga_xSe$ systems.

Fig. 1 presents the calculated electronic band structures of $In_{0.3}Ga_{0.7}Se$ obtained using the Perdew–Burke–Ernzerhof generalized gradient approximation (PBE-GGA) functional and the GGA+mBJ approach. Both computational schemes consistently predict a direct band-gap character, with the valence band maximum (VBM) and conduction band minimum (CBM) located at the Γ point of the Brillouin zone. The inclusion of the mBJ potential results in a pronounced widening of the band gap compared to the conventional GGA description. Within

the GGA+mBJ framework, the fundamental band gap is calculated to be approximately 1.91 eV. For comparison, previously reported experimental and theoretical studies indicate that the band gap of layered InSe is typically in the range of 1.2–1.3 eV, while GaSe exhibits a wider band gap of about 2.0–2.1 eV, depending on the polytype and computational approach. Intermediate compositions in the $In_xGa_{1-x}Se$ system have been shown to display a systematic increase in the band-gap energy with increasing Ga content. In this context, the calculated value of 1.91 eV for $In_{0.3}Ga_{0.7}Se$ is consistent with the expected compositional trend and confirms that non-equiatomic substitution provides an efficient route for continuous band-gap tuning in layered III–VI chalcogenide solid solutions. This value is intermediate between those reported for the binary compounds InSe and GaSe, reflecting the mixed cationic nature of the $In_{0.3}Ga_{0.7}Se$ solid solution. The result confirms that partial substitution of indium by gallium provides an effective route for tuning the electronic band structure and achieving controlled band-gap engineering in layered III–VI chalcogenides.

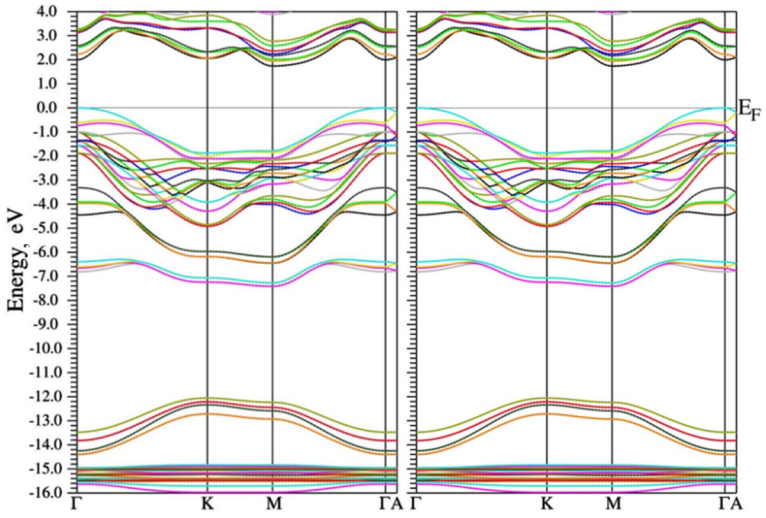

Fig. 1. Electronic band structures of the $In_{0.3}Ga_{0.7}Se$ crystal calculated using the PBE-GGA (left panel) and GGA+mBJ (right panel) exchange–correlation approaches. The Fermi level is set to zero energy.

To gain deeper insight into the electronic states governing the optical transitions, the atom-projected partial density of states (PDOS) calculated using the GGA+mBJ functional is shown in Fig. 2. The total density of states reflects the overall electronic structure of the crystal, while the atom-projected PDOS allows identification of the individual contributions of In, Ga, and Se atoms to the valence and conduction bands. The upper valence band region is dominated by p-orbital contributions from selenium atoms, with substantial hybridization with In-5p and Ga-4p states near the VBM. This hybridization reflects the covalent nature of bonding within the layers and plays a crucial role in determining the optical transition probabilities. The conduction band minimum is primarily composed of s-states originating from In and Ga atoms, with an additional contribution from Se-4p states. As a result, the fundamental optical transitions across the band gap are mainly of p–s character, which is consistent with the strong direct absorption observed in the calculated optical spectra. A distinct feature located at approximately −14 eV in the PDOS originates predominantly from Se-4s states and corresponds to deeper-lying bonding states that do not directly participate in optical transitions near the band edge.

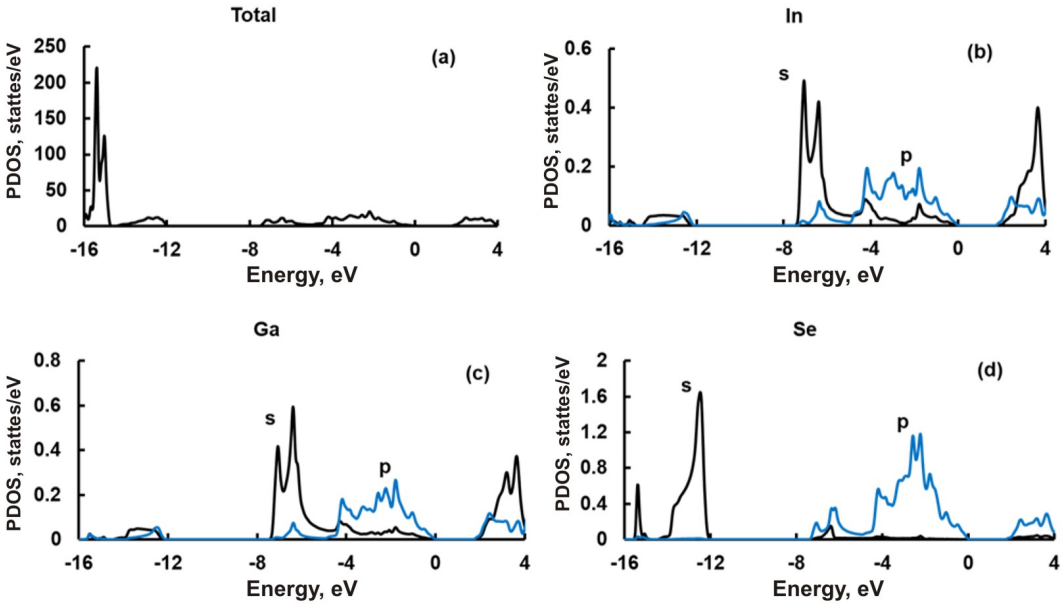

Fig. 2. Atom-projected partial density of states (PDOS) of $In_{0.3}Ga_{0.7}Se$ calculated within the GGA+mBJ approximation, with the Fermi level set to zero energy. Panel (a) shows the total density of states (TDOS), representing the sum of electronic states from all atoms and orbitals in the unit cell. Panels (b), (c), and (d) display the partial densities of states projected onto In, Ga, and Se atomic orbitals, respectively.

The frequency-dependent real and imaginary parts of the complex dielectric function of $In_{0.3}Ga_{0.7}Se$ are shown in Fig. 3 for light polarization perpendicular ($E \perp c$) and parallel ($E \| c$) to the optical axis, where the c axis is oriented normal to the crystallographic layers. The layered structure is characterized by strong in-plane covalent bonding within the *ab* plane and weak van der Waals interaction along the c direction; consequently, the natural cleavage plane is the (0001) plane, which is parallel to the *ab* plane. A pronounced optical anisotropy is evident, reflecting the layered crystal structure and the anisotropic bonding environment of $In_{0.3}Ga_{0.7}Se$. The in-plane imaginary component $\varepsilon_{\|}$ exhibits a strong peak centered near 5.53 eV, accompanied by weaker features at approximately 4.1 eV and 7.25 eV. These structures arise from interband transitions between hybridized In-5p/Ga-4p/Se-4p valence states and In-5s/Ga-4s-dominated conduction states, consistent with the PDOS analysis. The corresponding real part $\mathrm{Re}(\varepsilon_{\|})$ displays a characteristic dispersive behavior and crosses zero at higher photon energies, indicating the onset of collective electronic excitations in the ultraviolet region. In contrast, both the real and imaginary parts of the out-of-plane dielectric response ($E \| c$) are significantly weaker over the entire photon-energy range, reflecting the reduced electronic polarizability along the optical axis and the strong anisotropy inherent to the layered crystal structure.

Within the ultraviolet–visible spectral range, $In_{0.3}Ga_{0.7}Se$ demonstrates strong in-plane optical absorption, which can be attributed to the enhanced overlap of electronic wavefunctions within the layers. This behavior suggests that optical processes for light polarized parallel to the layers are considerably more efficient than those for light polarized perpendicular to the layers. At higher photon energies, the real part of the dielectric function becomes negative, with $\mathrm{Re}(\varepsilon_{\|})$ crossing zero at approximately 5.6 eV and $\mathrm{Re}(\varepsilon_{\perp})$ at about 6.9 eV. Consequently, an overall negative dielectric regime is observed in the energy window between roughly 5.6 and 6.9 eV, which is associated with enhanced reflectivity and plasmon-like features in the optical response.

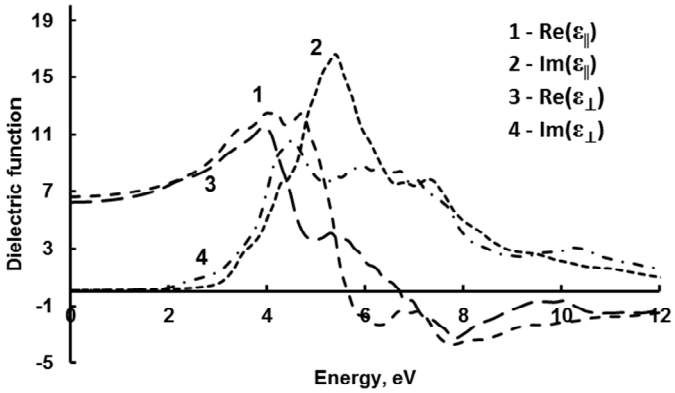

Fig. 3. Real and imaginary parts of the complex dielectric function of $In_{0.3}Ga_{0.7}Se$ for light polarized parallel ($\varepsilon_{\parallel}$) and perpendicular ($\varepsilon_{\perp}$) to the crystallographic layers.

The optical constants derived from the dielectric function, including the refractive index n, extinction coefficient k, absorption coefficient α, optical conductivity σ, and reflectivity R for light polarized parallel and perpendicular to the c-axis, are shown in Figs. 4–7. The refractive index spectra exhibit pronounced maxima in the near-ultraviolet region, with peak values reaching approximately 4, followed by a gradual decrease at higher photon energies. Below the fundamental absorption edge, the extinction coefficients remain negligible, while they increase sharply within the absorption bands. Throughout the considered energy range, the in-plane optical constants ($E \perp c$) exhibit substantially larger magnitudes than their out-of-plane counterparts ($E \parallel c$), further emphasizing the intrinsic anisotropy of the layered crystal structure. The static refractive indices, $n_{\perp}(0)$ and $n_{\parallel}(0)$, are both found to be close to 2.5, which is consistent with values reported for related layered chalcogenides.

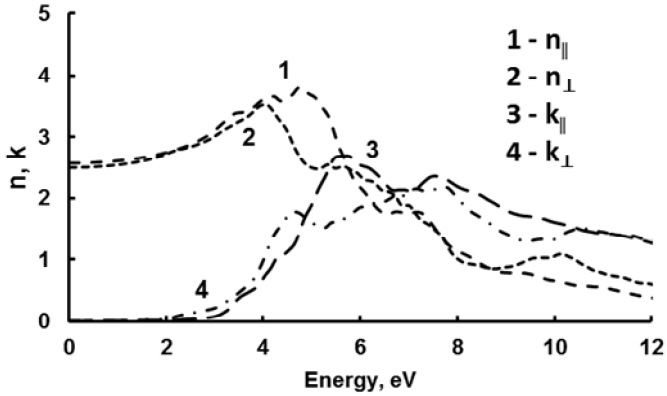

Fig. 4. Spectral dependences of the refractive index n and extinction coefficient k of $In_{0.3}Ga_{0.7}Se$ for different light polarizations. Curves 1 and 2 correspond to the refractive indices $n_{\parallel}$ and $n_{\perp}$, while curves 3 and 4 represent the extinction coefficients $k_{\parallel}$ and $k_{\perp}$ respectively. Here, the subscripts ∥ and ⊥ denote light polarization parallel ($E \parallel c$) and perpendicular ($E \perp c$) to the crystallographic c-axis.

The calculated absorption coefficient, shown in Fig. 5, reaches values on the order of 10^4–10^5 cm^{-1} in the photon-energy range of 2–8 eV. Such large absorption coefficients indicate strong direct, dipole-allowed interband transitions and confirm the suitability of $In_{0.3}Ga_{0.7}Se$ for optoelectronic applications operating in the visible and near-ultraviolet regions. As illustrated in Fig. 6, the real part of the optical conductivity remains negligible below the absorption edge and then increases sharply, exhibiting several pronounced peaks

in the energy range of approximately 4.6–7.5 eV. The most intense feature appears in the optical conductivity for polarization perpendicular to the c-axis ($E \perp c$) between 4 and 6 eV, and carries the dominant spectral weight. A corresponding but weaker peak is observed for polarization parallel to the c-axis ($E \| c$), reflecting the reduced transition probability along the optical axis. These conductivity maxima are directly correlated with the prominent peak in Im($\varepsilon_\perp$) near 5.5 eV and are responsible for the rapid increase in absorption and reflectivity in the ultraviolet region. At photon energies exceeding 8 eV, the optical conductivity decreases and displays only minor secondary features, while the anisotropy between the two polarization directions becomes less pronounced.

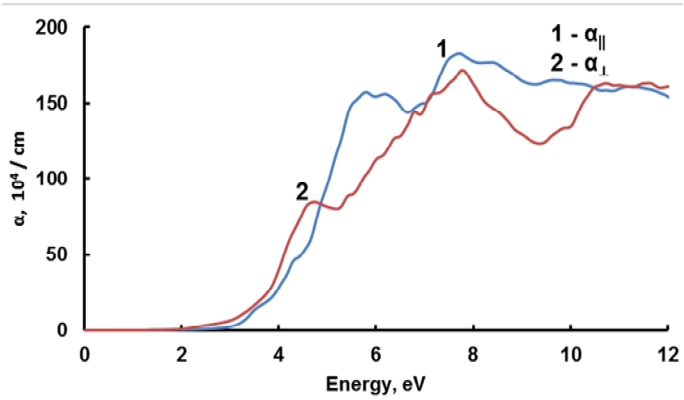

Fig. 5. Calculated absorption coefficient α of $In_{0.3}Ga_{0.7}Se$ as a function of photon energy for different light polarizations. The curves $\alpha_\|$ and $\alpha_\perp$ correspond to light polarized parallel ($E \| c$) and perpendicular ($E \perp c$) to the crystallographic c-axis, respectively.

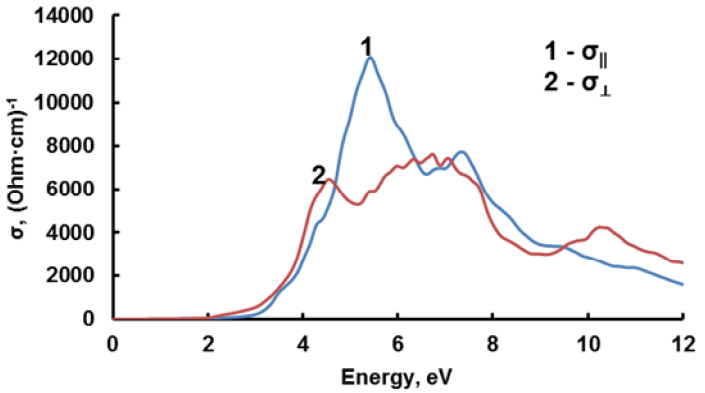

Fig. 6. Energy dependence of the real part of the optical conductivity σ. of $In_{0.3}Ga_{0.7}Se$ for light polarized parallel ($E \| c$) and perpendicular ($E \perp c$) to the crystallographic c-axis.

The reflectivity spectra for light polarized parallel ($R_\|$) and perpendicular ($R_\perp$) to the crystallographic c-axis are shown in Fig. 7. At photon energies below the fundamental band gap, both polarization components exhibit relatively low reflectivity values of approximately 0.2. With increasing photon energy, the reflectivity increases monotonically and reaches intermediate maxima of about 0.4–0.6 in the ultraviolet region, corresponding to the energy range of the most intense interband transitions. Additionally, less pronounced features appear at higher photon energies and are associated with deeper electronic transitions. Overall, the reflectivity behavior is fully consistent with trends observed in the dielectric function, optical conductivity, and absorption spectra, thereby confirming the internal consistency of the calculated optical response of $In_{0.3}Ga_{0.7}Se$.

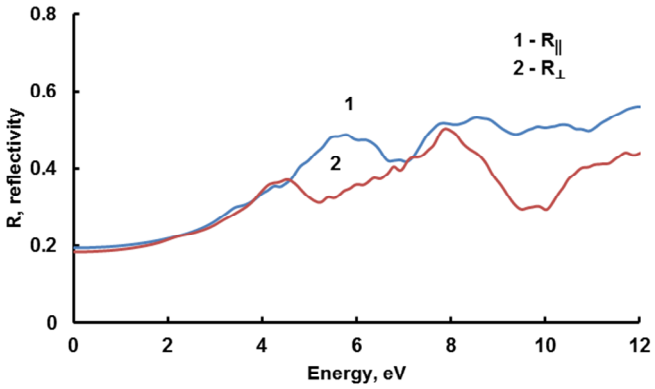

Fig. 7. Reflectivity spectra R of the $In_{0.3}Ga_{0.7}Se$ crystal for light polarized parallel ($R_{\parallel}$) and perpendicular ($R_{\perp}$) to the crystallographic c-axis, corresponding to light polarization $E \parallel c$ and $E \perp c$, respectively.

4.4. Dynamical and elastic properties

The compound $In_{0.3}Ga_{0.7}Se$ crystallizes in a primitive hexagonal structure with space group $P6_3$ mc (No. 186), corresponding to the C_{6v} (6mm) point-group symmetry. The primitive unit cell contains 16 atoms, which gives rise to a total of 48 phonon modes at the Brillouin-zone center. Within this structure, the In and Ga atoms occupy the Wyckoff 2*a* positions, while the Se atoms are located at the Wyckoff 2*b* positions. The group-theoretical decomposition of the vibrational modes at the Γ point is given by $\Gamma = 8A_1 + 8B_1 + 8E_2 + 8E_1$. Among these modes, the acoustic contribution is $\Gamma_{acoustic} = A_1 + E_1$, while the remaining optical modes are given by $\Gamma_{optical} = 7A_1 + 8B_1 + 8E_2 + 7E_1$.

According to the symmetry selection rules for the $P6_3mc$ space group, the A_1, E_1, and E_2 modes are Raman-active. In addition, the polar A_1 and E_1 modes are also infrared-active, whereas the B_1 modes are silent. In terms of degeneracy, the A_1 modes are nondegenerate, while the E_1 and E_2 modes are doubly degenerate.

The symmetry analysis further indicates that the atomic displacements associated with the doubly degenerate E_1 and E_2 modes are confined to the basal plane of the crystal layers. In contrast, the displacements corresponding to the nondegenerate A_1 and B_1 modes are polarized along the crystallographic *c*-axis, perpendicular to the layers. Moreover, the vibrational patterns differ in phase: atoms belonging to the same basis vibrate in-phase for the A_1 and E_1 modes, while out-of-phase (antiparallel) atomic displacements are characteristic of the B_1 and E_2 modes. These symmetry-determined displacement patterns play a key role in defining the Raman and infrared activity of the phonon modes in layered III–VI chalcogenides.

The calculated phonon dispersion relations and the corresponding atom-projected phonon density of states of hexagonal $In_{0.3}Ga_{0.7}Se$, obtained from first-principles density-functional perturbation theory, are presented in Figs. 8 and 9, respectively. The absence of imaginary phonon frequencies throughout the Brillouin zone confirms the dynamical stability of the crystal structure. Fig. 10 displays the experimentally measured Raman spectrum of $In_{0.3}Ga_{0.7}Se$. A direct comparison between the experimentally observed Raman peaks and the theoretically calculated Γ-point optical phonon frequencies is provided in Table 1. The overall agreement between theory and experiment is favorable, supporting the reliability of the adopted computational approach.

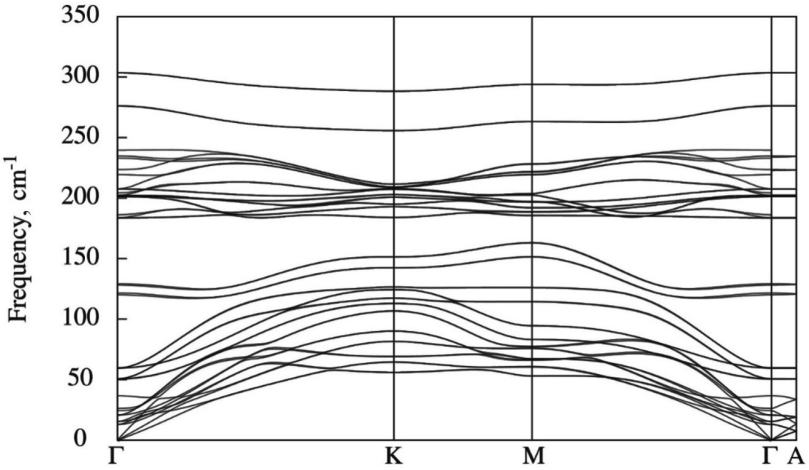

Fig. 8. Phonon dispersion relations of hexagonal $In_{0.3}Ga_{0.7}Se$.

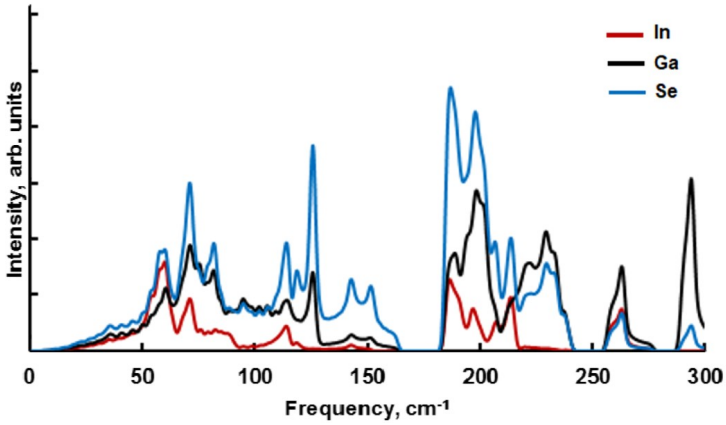

Fig. 9. Atom-projected phonon density of states of $In_{0.3}Ga_{0.7}Se$.

Table 1. Calculated and experimentally observed Γ-point optical phonon frequencies (cm^{-1}) of $In_{0.3}Ga_{0.7}Se$, together with mode symmetry and spectroscopic activity.

Mode symmetry	Spectroscopic activity	ω_{theo} (cm^{-1})	ω_{exp} (cm^{-1})	Mode symmetry	Spectroscopic activity	ω_{theo} (cm^{-1})	ω_{exp} (cm^{-1})
1	2	3	4	1	2	3	4
A_1	Raman, IR	37.0	40	E_1	Raman, IR	20.7	—
A_1	Raman, IR	118.0	111	E_1	Raman, IR	50.4	—
A_1	Raman, IR	129.2	—	E_1	Raman, IR	59.6	—
A_1	Raman, IR	219.4	225	E_1	Raman, IR	183.7	180
A_1	Raman, IR	234.7	—	E_1	Raman, IR	201.3	—
A_1	Raman, IR	266.0	256	E_1	Raman, IR	202.3	—
A_1	Raman, IR	303.4	—	E_1	Raman, IR	276.0	—
B_1	Silent	24.3	—	E_2	Raman	13.0	—
B_1	Silent	26.1	—	E_2	Raman	15.4	—
B_1	Silent	121.5	—	E_2	Raman	50.8	—
B_1	Silent	128.1	—	E_2	Raman	59.5	—
B_1	Silent	223.5	—	E_2	Raman	183.7	—
B_1	Silent	233.0	—	E_2	Raman	201.5	—
B_1	Silent	276.3	—	E_2	Raman	202.5	—
B_1	Silent	303.5	—	E_2	Raman	207.6	—

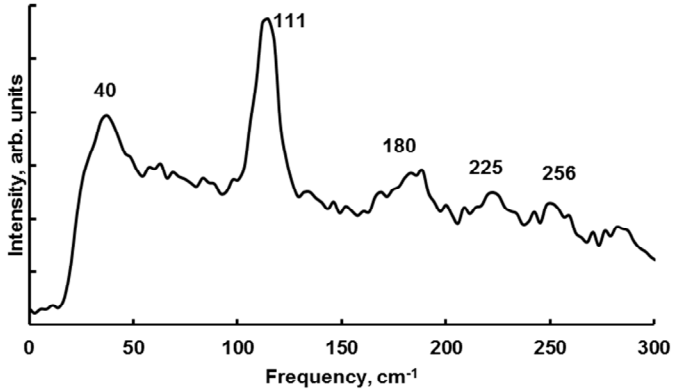

Fig. 10. Experimental Raman spectrum of hexagonal $In_{0.3}Ga_{0.7}Se$ measured at room temperature in a backscattering configuration.

An analysis of the phonon eigenvectors, together with the atom-projected phonon density of states shown in Fig. 9, reveals that the vibrational spectrum of $In_{0.3}Ga_{0.7}Se$ can be divided into several characteristic frequency regions. The low-frequency range (0–150 cm^{-1}), which includes the acoustic branches and the lowest optical modes, is dominated by vibrations involving In and Se atoms and exhibits pronounced peaks near 60, 72, and 114 cm^{-1}. The upper part of this region (100–150 cm^{-1}), with features around 114 and 140 cm^{-1}, originates mainly from Se atomic displacements, with a secondary contribution from In atoms. A separate mid- to high-frequency region is also largely governed by Se vibrations. In contrast, the highest-frequency phonon band, characterized by a peak near 259 cm^{-1}, is predominantly associated with vibrations of the lighter Ga atoms. This clear separation of vibrational contributions reflects the mass difference between the constituent elements and the layered crystal structure.

The elastic properties provide essential information on the effective interatomic bonding and mechanical response of the crystal and are closely related to its vibrational and thermodynamic behavior. In hexagonal crystals, the elastic tensor is fully described by five independent elastic constants: C_{11}, C_{12}, C_{13}, C_{33}, and C_{44}. The mechanical stability of a hexagonal lattice is governed by the Born–Huang stability criteria, which require the following conditions to be satisfied [28]: $C_{11} > |C_{12}|$, $C_{44} > 0$, and $(C_{11} + C_{12})C_{33} > 2C_{13}^2$.

The calculated elastic constants of $In_{0.3}Ga_{0.7}Se$ are C_{11}=96.3 GPa, C_{12}=27.3 GPa, C_{13}=14.2 GPa, C_{33}=36.3 GPa, and C_{44}=11.3 GPa. These values satisfy the Born–Huang mechanical stability criteria for a hexagonal lattice, namely $C_{11}>|C_{12}|$, $C_{44}>0$, and $(C_{11}+C_{12})C_{33}>2C_{13}^2$, confirming the mechanical stability of the crystal. The relatively larger in-plane elastic constants compared to the out-of-plane ones are consistent with the layered crystal structure, indicating stronger bonding within the layers and weaker interlayer interactions along the *c*-axis.

The constant-volume molar heat capacity C_V of $In_{0.3}Ga_{0.7}Se$ was derived from the calculated phonon spectrum, as shown in Fig. 11. At low temperatures (below approximately 5 K), the heat capacity follows the characteristic Debye T^3 dependence, reflecting the dominance of acoustic phonon contributions. With increasing temperature, C_V rises rapidly and approaches a value of approximately 390 J mol^{-1} K^{-1} at 400 K. This value is close to the classical Dulong–Petit limit of about 398 J mol^{-1} K^{-1} expected for this compound, indicating that all vibrational degrees of freedom become thermally activated at high temperatures.

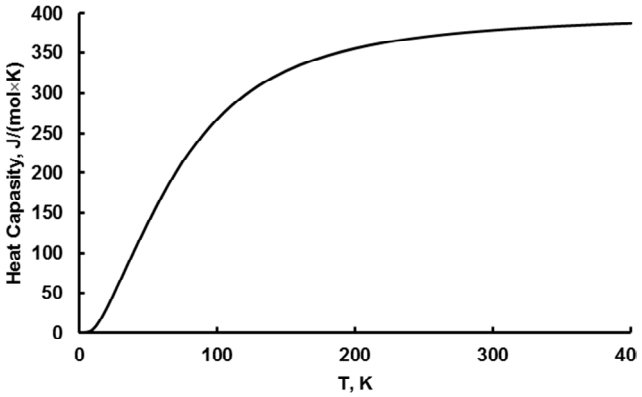

Fig. 11. Constant-volume heat capacity C_V of $In_{0.3}Ga_{0.7}Se$ as a function of temperature, expressed in units of $J \times mol^{-1}\ K^{-1}$.

5. Conclusion

The electronic structure, optical response, lattice dynamics, elastic behavior, and thermodynamic properties of the layered semiconductor $In_{0.3}Ga_{0.7}Se$ have been systematically investigated using first-principles density functional theory, complemented by experimental Raman spectroscopy. The electronic band structure calculations performed within the GGA+mBJ exchange–correlation framework demonstrate that $In_{0.3}Ga_{0.7}Se$ is a direct-gap semiconductor with a fundamental band gap of approximately 1.9 eV, positioning this non-equiatomic solid solution as a promising candidate for optoelectronic applications operating in the visible spectral range.

Analysis of the atom-projected partial density of states provides detailed insight into the bonding and electronic transition mechanisms. The upper valence band is dominated by hybridized p-states of In (5p), Ga (4p), and Se (4p), with Se-4p orbitals contributing most strongly near the valence-band maximum. In contrast, the conduction band minimum is primarily composed of In-5s and Ga-4s states, with a minor admixture of Se-4p character. This pronounced p–s nature of the band-edge states governs the direct optical transitions responsible for the strong absorption observed in the calculated optical spectra. A distinct spectral feature located around −14 eV in the density of states originates predominantly from localized Se-4s states, corresponding to deeper bonding states that do not participate directly in low-energy optical processes.

The vibrational properties of $In_{0.3}Ga_{0.7}Se$ were explored through density-functional perturbation theory and validated by Raman spectroscopy. The calculated Γ-point phonon frequencies exhibit satisfactory agreement with the experimentally observed Raman modes, confirming the reliability of the adopted computational approach. The atom-projected phonon density of states reveals that the low-frequency vibrational spectrum is primarily associated with collective motions of In and Se atoms, while the higher-frequency part of this region is dominated by Se displacements with a secondary contribution from In. The highest-frequency optical mode, observed near 259 cm^{-1}, is attributed mainly to vibrations of Ga atoms, reflecting the lighter atomic mass of gallium relative to indium.

A detailed analysis of the phonon eigenvectors further clarifies the symmetry and polarization characteristics of the vibrational modes. The doubly degenerate E_1 and E_2 modes involve atomic displacements confined within the basal plane of the crystal layers,

whereas the nondegenerate A_1 and B_1 modes correspond to out-of-plane vibrations polarized along the crystallographic *c*-axis. With respect to phase relations, atoms within the primitive-cell basis vibrate in-phase for the A_1 and E_1 modes, while antiparallel, out-of-phase displacements characterize the B_1 and E_2 modes. These symmetry-dependent displacement patterns account for the observed Raman and infrared activity of the phonon modes in this layered III–VI chalcogenide.

The calculated elastic constants satisfy all Born mechanical stability criteria for a hexagonal lattice, confirming the mechanical stability of $In_{0.3}Ga_{0.7}Se$. The pronounced difference between the in-plane and out-of-plane elastic responses reflects the intrinsic structural anisotropy of the layered crystal and is consistent with the anisotropic phonon and optical properties. Furthermore, the temperature-dependent constant-volume heat capacity derived from the phonon spectrum exhibits the expected Debye T^3 behavior at low temperatures and approaches the classical Dulong–Petit limit at high temperatures, indicating full activation of vibrational degrees of freedom.

Overall, this comprehensive study demonstrates that partial substitution of indium by gallium in layered In–Ga–Se compounds provides an effective strategy for tailoring electronic, optical, and vibrational properties. The combined theoretical and experimental results presented here establish $In_{0.3}Ga_{0.7}Se$ as a mechanically stable, optically active, and anisotropic semiconductor.

Funding. This research did not receive any specific grant from funding agencies in the public, commercial, or not-for-profit sectors.

Conflict of interest. The authors declare that they have no known competing financial interests or personal relationships that could have appeared to influence the work reported in this paper.

References

1. Huang, W., Gan, L., Li, H., Ma, Y., & Zhai, T. (2016). 2D layered group IIIA metal chalcogenides: synthesis, properties and applications in electronics and optoelectronics. *CrystEngComm*, *18*(22), 3968-3984.
2. Srivastava, R. P., Ranjan, P., Kumar, M., & Katiyar, A. K. (2025). 2D materials in functional optoelectronics: recent advances and future prospects. *Nanotechnology*, *36*(39), 392001.
3. Giri, A., Park, G., & Jeong, U. (2023). Layer-structured anisotropic metal chalcogenides: recent advances in synthesis, modulation, and applications. *Chemical Reviews*, *123*(7), 3329-3442.
4. Emir, C., Tataroglu, A., Coskun, E., & Bilge Ocak, S. (2024). Structural and optical properties of interfacial InSe thin film. *Acs Omega*, *9*(7), 7588-7596.
5. Bassou, A., Rajira, A., El Kanouny, A., Abounadi, A., El Haskouri, J., & Almaggoussi, A. (2021). Optical properties of GaSe, characterization and simulation. *Materials Today: Proceedings*, *37*, 3789-3792.
6. Liang, W. Y. (1973). Optical properties of layered compounds. *Journal of Physics C: Solid State Physics*, *6*, 551–559.
7. Sato, Y., Tang, C., Watanabe, K., Nakajima, M., Yamamoto, T., Tezuka, N., Tanabe, T. & Oyama, Y. (2021). Optical and Electrical Properties of $In_xGa_{1-x}Se$ Mixed Crystal Grown from Indium Flux by Traveling Heater Method. *Journal of Electronic Materials*, *50*(5), 2649-2655.
8. Yang, L., Zhou, G. J., & Lin, C. G. (2023). Composition-dependent properties and network structure of Ge-Se-Te chalcogenide glasses. *Chalcogenide Lett.*, *20*(1), 1-9.
9. Ning, C. Z., Dou, L., & Yang, P. (2017). Bandgap engineering in semiconductor alloy nanomaterials with widely tunable compositions. *Nature Reviews Materials*, *2*(12), 1-14.
10. Mammadova, G. N., Nurubeyli, T. K., Gulieva, S. O., Azizova, K. K., & Zeynalova, S. J. (2025). Dielectric and Optical Properties of Au-Doped $TlInSe_2$ for Advanced Optoelectronic Devices. *Physica B: Condensed Matter*, 417900.
11. Molina-Sanchez, A., & Wirtz, L. (2011). Phonons in single-layer and few-layer MoS_2 and WS_2. *Physical Review B – Condensed Matter and Materials Physics*, *84*(15), 155413.
12. Hasan, M., & Hossain, A. A. (2022). First-principles calculations to investigate the structural, electronic, optical anisotropy, and bonding properties of a newly synthesized ThRhGe equiatomic ternary intermetallic superconductor. *Results in Physics*, *42*, 106004.
13. Yi, J. X., Zhang, R. Z., Zhang, Y. Y., & Du, S. X. (2024). First-principle study of the electronic structure of layered Cu_2Se. *Journal of Physics: Condensed Matter*, *36*(5), 055501.

14. Alsalama, M. M., Hamoudi, H., Abdala, A., Ghouri, Z. K., & Youssef, K. M. (2020). Enhancement of thermoelectric properties of layered chalcogenide materials. *Reviews on Advanced Materials Science*, *59*(1), 371-378.
15. Jahangirli, Z. A., Asadullayeva, S. G., Amiraslanov, I. R., Eyyubov, Q. Y., Rahimli, A. B., & Abiyev, A. S. (2025). *Ab initio* and experimental investigations of the electronic and optical properties of pure and p-aminopyridine-intercalated $In_{1.2}Ga_{0.8}S_3$. *Indian Journal of Physics*, *99*, 2087–2092.
16. Azizova, K. K., Jahangirli, Z. A., Ragimov, S. S., Nurubeyli, T. K., Suleymanova, L. C., Kerimli, N., Mammadova, G. N., Mammadov, L., & Gulieva, S. O. (2025). Ab initio calculations of the electronic structure and optical properties of Cu_4SeTe crystals. *Ukrainian Journal of Physical Optics*, *26*(4), 4049–4057.
17. Jahangirli, Z. A., Rahimli, A. B., Mehdiyev, B. H., Seidov, R. G., Bayramova, T. O., Osmanova, S. S., & Guliyev, J. A. (2025). Electronic structure and optical properties of layered chalcogenides. *Physics of the Solid State*, *67*(5), 373–377.
18. Blaha, P., Schwarz, K., Tran, F., Laskowski, R., Madsen, G. K., & Marks, L. D. (2020). WIEN2k: An APW+ lo program for calculating the properties of solids. *The Journal of Chemical Physics*, *152*(7).
19. Blöchl, P. E., Jepsen, O., & Andersen, O. K. (1994). Improved tetrahedron method for Brillouin-zone integrations. *Physical Review B*, *49*(23), 16223.
20. Perdew, J. P., Burke, K., & Ernzerhof, M. (1996). Generalized gradient approximation made simple. *Physical Review Letters*, *77*(18), 3865.
21. Tran, F., & Blaha, P. (2009). Accurate band gaps of semiconductors and insulators with a semilocal exchange-correlation potential. *Physical Review Letters*, *102*(22), 226401.
22. Giannozzi, P., De Gironcoli, S., Pavone, P., & Baroni, S. (1991). Ab initio calculation of phonon dispersions in semiconductors. *Physical Review B*, *43*(9), 7231.
23. Baroni, S., de Gironcoli, S., Dal Corso, A., & Giannozzi, P. (2001). Phonons and related crystal properties from density-functional perturbation theory. *Reviews of Modern Physics*, *73*, 515–562.
24. Gonze, X. (1997). First-principles responses of solids to atomic displacements and homogeneous electric fields. *Physical Review B*, *55*, 10337–10354.
25. Gonze, X., & Lee, C. (1997). Dynamical matrices, Born effective charges, and dielectric permittivity tensors. *Physical Review B*, *55*, 10355–10368.
26. Gonze, X., Beuken, J.-M., Caracas, R., Detraux, F., Fuchs, M., Rignanese, G.-M., Sindic, L., Verstraete, M., Zerah, G., Jollet, F., Torrent, M., Roy, A., Mikami, M., Ghosez, Ph., Raty, J.-Y., & Allan, D. C. (2002). First-principles computation of material properties: The ABINIT project. *Computational Materials Science*, *25*, 478–492.
27. Nurubeyli, T., Hashimov, A., Nurubayli, Z., Nuriyev, K., & Imamverdiyev, N. (2025). Application of inductively coupled plasma mass spectrometry for geochemical analysis of rocks to enhance oil and gas production forecasting. *Mining of Mineral Deposits*, *19*(3), 43–50.
28. Hartwigsen, C., Goedecker, S., & Hutter, J. (1998). Relativistic separable dual-space Gaussian pseudopotentials. *Physical Review B*, *58*, 3641–3662.
29. Monkhorst, H. J., & Pack, J. D. (1976). Special points for Brillouin-zone integrations. *Physical Review B*, *13*, 5188–5192.
30. Mouhat, F., & Coudert, F.-X. (2014). Necessary and sufficient elastic stability conditions in various crystal systems. *Physical Review B*, *90*, 224104.
31. Amiraslanov, I. R., Azizova, K. K., Jahangirli, Z. A., Nabieva, S. A., Mammadov, F. M., Aliyeva, Y. R., Aliyeva, M. Kh., & Aliev, Z. S. (2021). Synthesis and characterization of new indium gallium selenides of the InSe–GaSe system. *Journal of Solid State Chemistry*, *304*, 122569.

Azizova, K. K., Jahangirli, Z. A., Nurubeyli, T. K., Suleymanova, L. Ch., Sultanova, A. H., Kerimli, N. V., Gulieva, S. O., Osmanova, S. S., Mammadov, L. V., Kazimova, N.V. (2026). Electronic, Optical, and Vibrational Properties of Layered $In_{0.3}Ga_{0.7}Se$: A DFT and Raman Study**.** *Ukrainian Journal of Physical Optics*, *27*(2), 02043 – 02057. doi: 10.3116/16091833/Ukr.J.Phys.Opt.2026.02043

Анотація. *Електронну структуру, оптичний відгук і коливальні властивості кристала $In_{0.3}Ga_{0.7}Se$ досліджено з використанням теорії функціоналу густини ab initio. Було розраховано компоненти тензора діелектричної функції, що дало змогу виконати детальний аналіз показника заломлення, коефіцієнта екстинкції, коефіцієнта поглинання, оптичної провідності та коефіцієнта відбивання для світла, поляризованого паралельно та перпендикулярно до оптичної осі. Отримані результати ідентифікують $In_{0.3}Ga_{0.7}Se$ як прямозонний напівпровідник із фундаментальною шириною забороненої зони 1,91 еВ, що підкреслює його потенціал для оптоелектронних застосувань у видимому спектральному діапазоні. Для з'ясування особливостей електронної структури було проаналізовано атомно-проєктовані парціальні густини станів, які виявили внески орбіталей In, Ga та Se у формуванні валентної зони та зони провідності. Коливальні властивості досліджено за допомогою комбінованого теоретичного та експериментального підходу з використанням теорії збурень*

функціоналу густини та раманівської спектроскопії. Пряме порівняння розрахованих фононних мод з експериментальним спектром комбінаційного розсіювання дало змогу ідентифікувати п'ять раман-активних мод із частотами 40, 111, 180, 225 та 256 $см^{-1}$, що відповідають симетрійним представленням A_1, B_1, E_2 та E_1. Відповідні картини атомних зміщень було проаналізовано для з'ясування природи коливань кристалічної ґратки в системі зі змішаними катіонами. Крім того, було розраховано температурну залежність теплоємності в інтервалі 0–400 К, що дало змогу охарактеризувати термодинамічну поведінку $In_{0.3}Ga_{0.7}Se$. Загальна узгодженість між розрахованими фононними частотами та експериментальними даними комбінаційного розсіювання підтверджує надійність ab initio підходу та забезпечує узгоджений опис електронних, оптичних, коливальних і термодинамічних властивостей цього нееквіатомного твердого розчину In–Ga–Se.

Ключові слова: *кристали $In_{0.3}Ga_{0.7}Se$, теорія функціоналу густини, електронна структура, оптична анізотропія, комбінаційна спектроскопія, фононні властивості*